CORA Cork Open Research Archive
Cartlann Taighde Oscailte Chorcaí

Title	Theoretical models for underwater RFID and the impact of water salinity on the design of wireless systems
Authors	Peres, Caroline;Pigeon, Melusine;Rather, Nadeem;Gawade, Dinesh R.;Buckley, John;Jafarzadeh, Hamed;O'Flynn, Brendan
Publication date	2020-12-30
Original Citation	Peres, C., Pigeon, M., Rather, N., Gawade, D., Buckley, J., Jafarzadeh, H. and O'Flynn, B. (2020) 'Theoretical Models for Underwater RFID and the Impact of Water Salinity on the Design of Wireless Systems', International Journal on Advances in Networks and Services, 13 (34), pp. 45-59.
Type of publication	Article (peer-reviewed)
Link to publisher's version	http://www.thinkmind.org/index.php?view=article&articleid=netser_v13_n34_2020_1
Rights	2020, © Copyright by authors, Published under agreement with IARIA - www.iaria.org
Download date	2026-11-01 09:32:01
Item downloaded from	https://hdl.handle.net/10468/11111

UCC
University College Cork, Ireland
Coláiste na hOllscoile Corcaigh

Theoretical Models for Underwater RFID and the Impact of Water Salinity on the Design of Wireless Systems

Caroline Peres, Melusine Pigeon, Nadeem Rather, Dinesh Gawade, John Buckley, Hamed Jafarzadeh, Brendan O'Flynn

Tyndall National Institute
University College Cork
Cork, Ireland

caroline.peres@tyndall.ie, melusine.pidgeon@tyndall.ie, nadeem.rather@tyndall.ie, dinesh.gawade@tyndall.ie, john.buckley@tyndall.ie, hamed.jafarzadeh@tyndall.ie, brendan.oflynn@tyndall.ie

***Abstract*— Underwater wireless communications present challenges due to the characteristics of water as a propagation channel medium. Regardless, wireless communications are needed for a range of systems that operate underwater. Commonly used technologies for these use cases (radio-frequency, acoustic and optical communications) are lacking, as they generally suffer from strong attenuation, multipath effects and propagation delays. In this context, we explore the theoretical models for Path Loss of Radio Frequency Identification (RFID) systems underwater in regards to the salinity of the water. We also discuss RFID systems feasibility in such applications as aquaculture and fish stock management. This paper aims to discuss the theoretical transmission models for RFID systems underwater, separating them into near-field systems – which use Magnetic Induction (MI) to communicate – and far-field systems – that transfer data via Radio Frequency (RF). We determine the path loss for each case, the effect of the salinity in the model for the path loss, and present preliminary measurements of magnetic field strength underwater for different salinity values.**

Keywords- RFID; underwater wireless communications; underwater RFID; near-field communication; magnetic induction; salinity.

I. INTRODUCTION

This paper is an extension of a previous conference submission [1]. Underwater wireless communications present some challenges due to the characteristics of the channel medium. The underwater environment has different characteristics and phenomena compared to those typical for terrestrial radio propagation channel [2]. Despite these difficulties, underwater wireless communications are needed for a variety of underwater systems. Practical applications include seismic activity monitoring, equipment monitoring and control, underwater wireless sensor networks, underwater robots and Underwater Autonomous Vehicles (UAVs), aquaculture, fish stock management and underwater environmental monitoring [3][4].

There are three commonly used technologies for underwater communications [2][5][6]. Radio-frequency (RF) communication consists of propagating electromagnetic waves, and it has high data rates at short ranges but suffers from multipath propagation, strong attenuation and Doppler effect [2]. Due to the increasing attenuation for higher frequencies, it requires that systems operate at lower frequencies to achieve longer ranges of transmission, which in turn demands the use of large antennas making it unsuitable for some applications. Acoustic communication makes use of propagating sound waves, which have low attenuation underwater, achieving the longest range [2]. However, this type of communication exhibits a large propagation delay due to the speed of sound underwater, suffers from multipath propagation, and is affected by a large delay spread that leads to inter-symbol interference. Temperature gradients and ambient noise are also problems for acoustic communications. Another technology that can be used for underwater use is optical communication, which uses electromagnetic waves in the visible spectrum to transmit data. Such technologies have large data rates with low propagation delay. However, they suffer severe absorption in water and strong backscatter due to turbidity (e.g., suspended particles in the medium) [2].

Underwater Radio-Frequency Identification (RFID) is not an extensively explored topic due to the problems outlined above for RF communications, specifically strong attenuation and multipath propagation. However, some RFID systems communicate via Magnetic Induction (MI), which could provide an alternative for the existing technologies [4][7]. In this paper, we want to explore the potential for such technology to be used in the marine environment. We examine the different methods of communication that different RFID systems employ, separating them into two categories: near-field communication and far-field communication. Theoretical mathematical models exist for terrestrial RFID systems, from which the system functionality, communication properties and link budget can be derived. This paper aims to derive similar models for underwater RFID communications, by describing the underwater channel physical properties for near-field and far-field electromagnetic fields by presenting the path loss for each. This can then be used to predict communication range, link budget and channel capacity.

2020, © Copyright by authors, Published under agreement with IARIA - www.iaria.org

This paper is organised as follows. Section II discusses the related work. In Section III, we give a brief overview of an RFID system and its components. Section IV then presents the model for underwater RFID for near-field and far-field communications. In Section V, we present preliminary results of measurements done of magnetic field strength in various water solutions of different salinity values. Section VI discusses underwater RFID in light of the theory presented and the measurement results. We conclude the paper in Section VII.

II. Related Work

Underwater RFID is not a common topic due to the challenges that the underwater environment poses to RF communications. However, some preliminary work has been done. For example, [8] explores the use of Near-Field Communication (NFC) underwater. Using smartphones and smart cards operating at 13.56 MHz, they tested the read range achieved and the influence of dissolved salts in water in the read range. Another group used Low-Frequency (LF) RFID to track the sediment movements in a beach [9]. Transponders were coupled to pebbles, creating "smart" pebbles that could be detected at up to 50 cm underwater. They were then released into the beach and tracked to map the sediment movement. Systems that use LF RFID underwater can be found in Passive Integrated Transponder (PIT) tags used to uniquely identify fish in fisheries and research [10][11].

The authors in [12] summarised the current understanding of underwater RFID, examining the penetration depth in freshwater and seawater. However, the model presented is simplified and accounts only for the far-field operation. They also showcase other uses of RFID underwater, such as underwater pipeline monitoring. Other authors have explored MI communications underwater, where the system communicates via induction coupling. [13] provides an overview of the current research findings and challenges for MI. Models for MI can be found in [14]–[18].

III. RFID System

A typical RFID system is comprised of a tag and a reader (initiator). The tag is used to identify or measure ambient parameters, typically temperature for instance [19]. Furthermore, a reader is used to read and write data from or into such tag located within its proximity or vicinity. The tag consists of a coupling or backscatter element such as a conductor loop or an antenna, and an RFID radio that stores the data or ultra-low-power embedded system to measure various ambient parameters and store relevant metadata. The reader also comprises similar antennas as a coupling element along with a control unit and an RFID radio. Generally, near-field RFID uses inductive coupling between the reader and tag loop antennas to communicate with each other when located within each other's proximity or vicinity. RFID operates at 120–135 kHz low frequency (LF) unregulated band and high frequency (HF) 13.56 MHz Industrial, Scientific, and Medical (ISM) band. LF RFID follows the ISO/IEC 18000-2 standard and HF RFID follows ISO/IEC 18000-3 standard along with additional smart cards ISO/IEC 15693, ISO/IEC 14443A and 14443B standard [20]–[24][25, p. 1][26]. Additional NFC standards ensure the interoperability of NFC-enabled devices and enable communication between them. The NFC standard defines the data rate (26.48 to 424 kbit/s), data frame formats such as NFC Data Exchange Format (NDEF), modulation, initialization, and collision control during initialization [27].

In Figure 1 the block diagram of a typical RFID sensing system is shown. The conductor loop antenna of the reader generates the magnetic alternating field. The magnetic flux (Φ) generated by the reader loop antenna is used as a power supply for the sensor tag. This is achieved by utilising the voltage which is induced in the tag antenna by mutual inductance (*M*) between the transmitter and receiver antenna. Due to this induced voltage, a current starts flowing in the tag antenna and its value can be theoretically calculated from the quotient of the voltage divided by the impedance of the tag antenna [28]. Furthermore, the NFC radio Analog Front End (AFE) consists of an RF interface and the energy harvesting circuitry, which will connect to the loop antenna. The harvested voltage will further be regulated using a low dropout regulator and will be used to power up an ultra-low-power Microcontroller Unit (MCU), as well as a sensor [28]. The NFC radio consist of an Amplitude Shift Keying (ASK) demodulator which will demodulate the messages from the reader and responds to the reader with the help of load modulation. The load modulation is achieved by varying the impedance of the tag antenna [28]. The NFC radio and sensor will be interfaced with MCU using the Inter-Integrated Circuit (I2C) Protocol. The sensor will start sensing a parameter and its raw value will be transmitted to the MCU through the I2C. The MCU will then generate an NDEF message with the sensed value and forward it to the NFC radio [19][29].

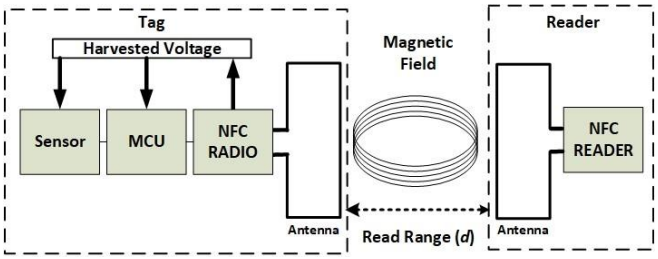


Figure 1. Block diagram of a RFID sensing system.

The tag receives the signal via the coupling element, and utilises the induced voltage to power up the tag's RFID radio and other electronics. RFID radio then sends data back to the reader via load modulation or backscatter. In general, such a tag is battery-less, and it is powered by the Magnetic flux (Φ) generated by the reader. Other battery assisted power (BAP) system models exist incorporating an active RFID device that

2020, © Copyright by authors, Published under agreement with IARIA - www.iaria.org

consist of a battery as a power source. The added battery is used to power up additional tag electronics or sensors and to extend the communication distance range between the transmitter and receiver.

Equation (1) shows the relationship between the quality factor of the antenna *Q*, the bandwidth (*BW*) and the resonant frequency (*f*) for the system. For example, larger bandwidth is required to cover the sidebands of communication for the ISO/IEC 14443B standard and is particularly important to have if using higher data rates such as 424 or 848 kbps. In addition, for other applications based on the ISO/IEC15693 standard, the Q factor can be significantly higher, as the sidebands do not need such a wide bandwidth [30].

$$Q = f / BW \qquad (1)$$

IV. RFID Channel Physical Characteristics

The antenna or coil of the RFID reader generates an electromagnetic field. These fields can be described as time-harmonic fields in a lossy medium [31]:

$$\nabla^2 \boldsymbol{E} = \gamma \boldsymbol{E} \qquad (2)$$

$$\nabla^2 \boldsymbol{H} = \gamma \boldsymbol{H} \qquad (3)$$

where γ is the propagation wave number, with α as the attenuation and β as the phase variables. The wavelength λ is λ=2π/β.

$$\gamma = \alpha + j\beta = \sqrt{j\omega\mu(\sigma + j\omega\varepsilon)} \qquad (4)$$

$$\alpha = \omega\sqrt{\mu\varepsilon}\left[\frac{1}{2}\left(\sqrt{1+\left(\frac{\sigma}{\omega\varepsilon}\right)^2}-1\right)\right]^{1/2} \quad \left(\frac{Np}{m}\right) \qquad (5)$$

$$\beta = \omega\sqrt{\mu\varepsilon}\left[\frac{1}{2}\left(\sqrt{1+\left(\frac{\sigma}{\omega\varepsilon}\right)^2}+1\right)\right]^{1/2} \quad \left(\frac{rad}{m}\right) \qquad (6)$$

The magnetic permeability $\mu = \mu_0 = 4\pi \cdot 10^{-7}\mathrm{H/m}$ of the medium does not change for non-magnetic media. σ is the conductivity of the medium, which in this case is dependent on the salinity of the water, its temperature and pressure. The salinity of the water is proportional to the concentration of dissolved salts (chloride, sodium, sulphate, etc.). In marine water, the conductivity ranges from 2 S/m to 6 S/m for frequencies lower than 10 GHz, being considered constant 4 S/m in most cases [12]. In freshwater, the considerations are the same. However, the salinity is lower, which means that the conductivity is lower (typically ranging from 30 to 2000 μS/cm) [12]. Due to this high conductivity, Eddy currents are induced within the water, caused by the propagating magnetic field [32]. These Eddy currents are a source of attenuation of the magnetic field.

The conversion between salinity and conductivity for seawater has been defined in the practical-salinity-scale PSS-78 [33]. This scale defines a standard ratio between any measured combination of salinity, conductivity, and temperature in relation to a standard value of conductivity and temperature for seawater of salinity 35 *g*/*Kg*.

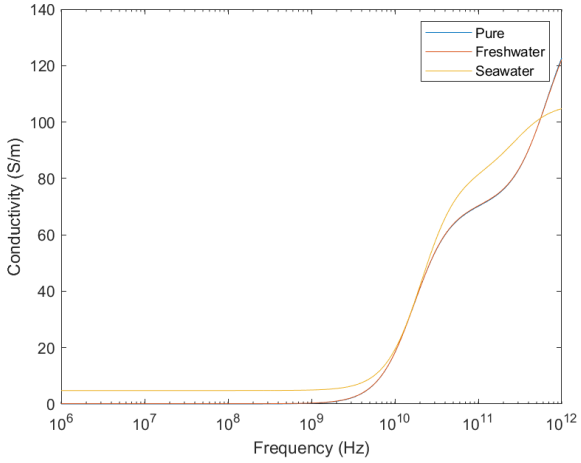


Figure 2: Conductivity of pure, freshwater and seawater for different values of propagating frequencies.

The dielectric permittivity of the medium ε is defined by $\varepsilon = \varepsilon_r\varepsilon_0$, $\varepsilon_0 = 8.854 \times 10^{-12}\mathrm{F/m}$being the permittivity in free-space and ε_r the relative permittivity of the medium. This relative permittivity is dependent on the composition of the medium that is polarised when placed under an electric field [34][35]. Equation (7) shows the relationship between the relative permittivity and the frequency of the propagating electromagnetic wave for pure water as modelled by Debye [35].

$$\varepsilon_r(\omega) = \varepsilon_\infty + \frac{\varepsilon_S - \varepsilon_\infty}{1 + j\omega\tau} \qquad (7)$$

In this equation, τ is a time constant of the exponentially increasing orientation polarisation called relaxation time, and ε_S and ε_∞ are the static and infinite frequency relative permittivities of the medium. All these parameters are dependent on the temperature.

However, for freshwater and seawater, due to the interaction between molecules and the presence of ions that increase the conductivity of the medium, the simple model is not enough to accurately predict the permittivity [34].

For freshwater, there are extensive experimental studies and various models that predict the dielectric permittivity [36]–[40].

Work has been done by [38][41]–[43] to empirically determine a model for the relative permittivity of seawater, but some results disagree with each other. The International Telecommunication Union released a recommendation [44] that advises the model to use when calculating the dielectric permittivity and conductivity of seawater based on its

2020, © Copyright by authors, Published under agreement with IARIA - www.iaria.org

salinity, which will be used in this paper. Equation (8) shows how to calculate the relative dielectric permittivity based on this model.

$$\varepsilon_r = \frac{\varepsilon_{SS}-\varepsilon_{1S}}{1+(f_{GHz}/f_{1S})^2} + \frac{\varepsilon_{1S}-\varepsilon_{\infty S}}{1+(f_{GHz}/f_{2S})^2} + \varepsilon_{\infty S} \quad (8)$$

The following equations show the calculations for each of the parameters from Equation (8).

$$\varepsilon_{SS} = \varepsilon_S exp(-3.33330 \times 10^{-3} S + 4.74868 \times 10^{-6} S^2) \quad (9)$$

$$f_{1S} = f_1\left(1 + S(2.3232 \times 10^{-3} - 7.9208 \times 10^{-5} T + 3.6764 \times 10^{-6} T^2 + 3.5594 \times 10^{-7} T^3 + 8.9795 \times 10^{-9} T^4)\right) \quad (10)$$

$$\varepsilon_{1S} = \varepsilon_1 exp(-6.28908 \times 10^{-3} S + 1.76032 \times 10^{-4} S^2 - 9.22144 \times 10^{-5} TS) \quad (11)$$

$$f_{2S} = f_2\left(1 + S(-1.99723 \times 10^{-2} + 1.81176 \times 10^{-4} T)\right) \quad (12)$$

$$\varepsilon_{\infty S} = \varepsilon_\infty\left(1 + S(-2.04265 \times 10^{-3} + 1.57883 \times 10^{-4} T)\right) \quad (13)$$

$$\varepsilon_S = 77.66 + 103.3 \quad (14)$$

$$\varepsilon_1 = 0.0671\varepsilon_S \quad (15)$$

$$\varepsilon_\infty = 3.52 - 7.52 \quad (16)$$

$$\Theta = \frac{300}{T+273.15} - 1 \quad (17)$$

$$f_1 = 20.20 - 146.4\Theta + 316\Theta^2 \quad (18)$$

$$f_2 = 39.8 f_1 \quad (19)$$

in which T is the temperature in degrees Celsius (°C), f_{GHz} is the frequency of the signal in GHz, S is the salinity in g/kg or ppt, and f_1 and f_2 are the Debye relaxation frequencies for pure water.

From the same model, the conductivity is:

$$\sigma = \sigma_{35} R_{35} R_{T15} \quad (S/m) \quad (20)$$

The following equations show the calculations for each of the parameters from Equation (20).

$$\sigma_{35} = 2.903602 + 8.607 \times 10^{-2} T + 4.738817 \times 10^{-4} T^2 - 2.991 \times 10^{-6} T^3 + 4.3047 \times 10^{-9} T^4 \quad (21)$$

$$R_{35} = S\frac{(37.5109+5.45216S+1.4409\times10^{-2}S^2)}{(1004.75+182.283S+S^2)} \quad (22)$$

$$R_{T15} = 1 + \frac{a_0(T-15)}{a_1+T} \quad (23)$$

$$a_0 = \frac{(6.9431+3.2841S-9.9486\times10^{-2}S^2)}{(84.850+69.024S+S^2)} \quad (24)$$

$$a_1 = 49.843 - 0.2276S - 0.198 \times 10^{-2} S^2 \quad (25)$$

Figure 2 shows the influence of the frequency of the signal in the conductivity of the medium. Figure 3 shows the complex permittivity for pure water, freshwater and seawater as a function of the frequency according to Equation (26).

$$\hat{\varepsilon} = \varepsilon_r - j\varepsilon_r'' = \frac{\varepsilon}{\varepsilon_0} - j\frac{\sigma}{\omega\varepsilon_0} \quad (26)$$

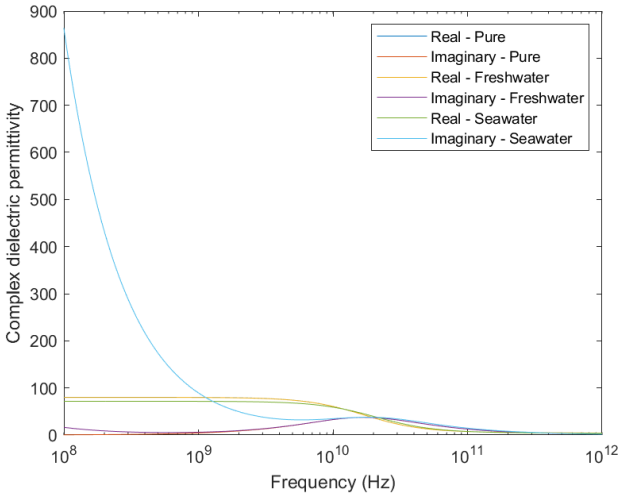


Figure 3: Real (relative permittivity) and imaginary parts of the complex dielectric permittivity for pure water, freshwater (Salinity = 0.5 g/kg) and seawater (Salinity = 35 g/kg) at temperature T = 20°C.

The dielectric permittivity and the conductivity are then used to determine the attenuation factor α. In [45], the authors propose a review of this model to account for the difference between the theoretical calculations and the empirical data of the attenuation of radio waves underwater. The experiments show that the signal attenuation at higher distances (≫10 m) is not as strong as predicted. Therefore, they redefine α as a corrected absorption factor α' that matches experimental results closely:

$$\alpha' = \alpha\left(\frac{\lambda}{\lambda+z}\right) \quad (27)$$

For the Transverse Electromagnetic Mode to the positive z direction in lossy medium (in this case, water), **E** and **H** can be derived as [31]:

$$\boldsymbol{E}(\boldsymbol{z}) = \hat{\boldsymbol{a}}_{\boldsymbol{x}} E_0 e^{-\gamma z} \quad (28)$$

$$\boldsymbol{H}(\boldsymbol{z}) = \hat{\boldsymbol{a}}_{\boldsymbol{y}} \frac{\gamma}{j\omega\mu} E_0 e^{-\gamma z} \quad (29)$$

2020, © Copyright by authors, Published under agreement with IARIA - www.iaria.org

For a given antenna, the space that surrounds it can be separated into three regions: (a) a reactive near-field, (b) a radiating near-field and (c) the far-field. There are no abrupt changes at their boundaries [46]. A representation of these regions can be seen in Figure 4.

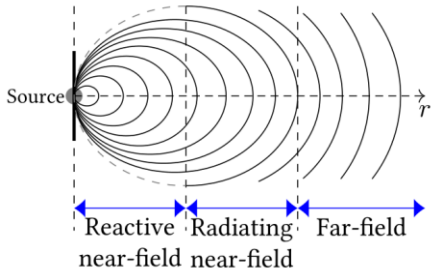


Figure 4: Field regions for a propagating electromagnetic wave leaving an antenna.

The *Reactive Near-Field* is the space immediately near the antenna where the reactive field predominates (magnetic field). For most antennas, the limit of this region is at $0.62\sqrt{D^3/\lambda}$ [46], where D is the biggest dimension of the antenna. The *Radiating Near-Field* is located between the reactive near-field and the far-field and is the space wherein radiation fields are dominant. The angular field distribution is determined by the distance from the antenna. This field existence depends on the ratio between antenna size D and the wavelength λ: if $D/\lambda \ll 1$ then this region does not exist. The *Far-Field* is the region wherein the electrical and magnetic components of the field become orthogonal to each other as they separate from the antenna and propagate as an electromagnetic wave. The lower boundary of this region is located at $2D^2 / \lambda$ for any antenna [31], also considered to be $\lambda/2\pi$ for dipole antennas. According to [28], a good approximate rule for RFID systems is to place the beginning of the far-field at $\lambda/2\pi$.

The field boundary distance is different for each medium due to the difference in wavelength. Tables I and II show the values for the attenuation coefficient, wavelength, and far-field boundary for freshwater and seawater, respectively.

Current RFID systems can be separated into two categories: near-field systems that work with inductive coupling due to the dominance of the magnetic field in the near-region, and far-field systems that receive power from the propagating electromagnetic waves in the far-field [47]. The frequencies used in each region are different. Since the lower frequencies – such as Low Frequency (LF) at around 134.2kHz and High Frequency (HF) at 13.56MHz – have a far-field boundary that is further away, they are mainly used in inductive coupling systems. Higher frequencies are then used mostly in far-field systems.

TABLE I. VALUES OF ATTENUATION FACTOR A, WAVELENGTH Λ AND FAR-FIELD BOUNDARY $z_F = \lambda/2$ FOR FRESHWATER (S = 0.5 G/KG).

Frequency	**α (Np/m)**	**λ (m)**	**z_F (m)**
134.2 kHz	2.16E-01	2.89E+01	4.60E+00
13.56 MHz	1.58E+00	2.10E+00	3.34E-01
433.9 MHz	2.83E+00	7.73E-02	1.23E-02
915 MHz	6.16E+00	3.67E-02	5.84E-03
1.5 GHz	1.34E+01	2.24E-02	3.57E-03
2.4 GHz	3.11E+01	1.41E-02	2.24E-03
5 GHz	1.24E+02	6.91E-03	1.10E-03

TABLE II. VALUES OF ATTENUATION FACTOR A, WAVELENGTH Λ AND FAR-FIELD BOUNDARY $z_F = \lambda/2$ FOR SEAWATER (S = 35 G/KG).

Frequency	α (Np/m)	λ (m)	z_F (m)
134.2 kHz	1.59E+00	3.94E+00	6.27E-01
13.56 MHz	1.59E+01	3.90E-01	6.20E-02
433.9 MHz	7.63E+01	5.80E-02	9.22E-03
915 MHz	9.51E+01	3.34E-02	5.32E-03
1.5 GHz	1.07E+02	2.19E-02	3.49E-03
2.4 GHz	1.25E+02	1.42E-02	2.27E-03
5 GHz	2.01E+02	7.08E-03	1.13E-03

A. *Near-field*

In the near-field, the magnetic field created by the reader's antenna induces a voltage in the transponder immersed in this field. This is called *inductive coupling* and the interaction between reader and transponder can be considered as coupled inductors. This method of communication can also be called *Magnetic Induction (MI)*.

Consider the equivalent circuit for the inductively coupled system shown in Figure 5. The transmitter antenna is fed by a source with internal impedance Z_S and the receiver antenna is terminated by a load impedance Z_L. The transmitter coil antenna has a impedance of $Z_{TX} = R_{TX} + j\omega L_{TX} + 1/(j\omega C_{TX})$ and the receiver coil antenna is $Z_{RX} = R_{RX} + j\omega L_{RX} + 1/(j\omega C_{RX})$.

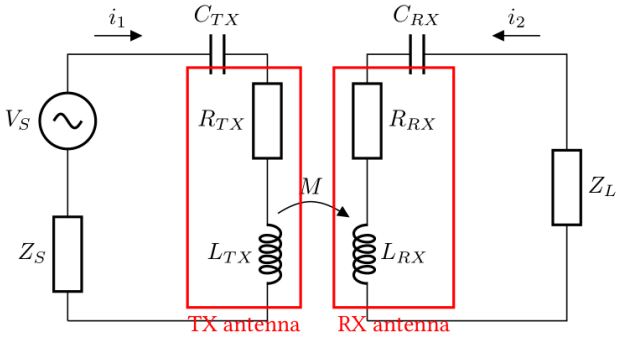


Figure 5: Inductive coupling between reader and transponder.

2020, © Copyright by authors, Published under agreement with IARIA - www.iaria.org

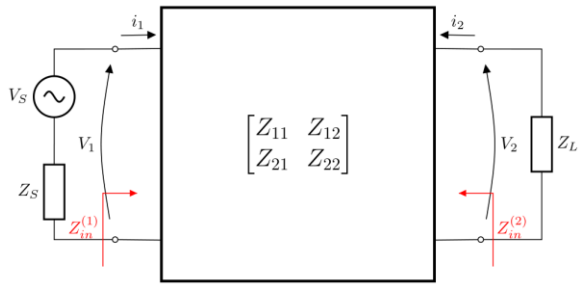


Figure 6: Two-port network equivalent of the system.

Using the two-port network equivalent (Figure 6) and considering an ideal source for V_S, $Z_{11} = Z_{TX}$ and $Z_{22} = Z_{RX}$ are the self-impedances of the coils and $Z_{12} = Z_{21} = j\omega M$ are the mutual impedances due to the coupling.

$$\begin{pmatrix} V_1 \\ -Z_L I_2 \end{pmatrix} = \begin{bmatrix} z_{11} & z_{12} \\ z_{21} & z_{22} \end{bmatrix} \cdot \begin{pmatrix} I_1 \\ I_2 \end{pmatrix} \quad (30)$$

The resistance of a coil is $R = N \cdot 2\pi a \cdot R_0$, where N is the number of turns of the coil, a is the diameter of the coil and R_0 is the resistance of a unit of length of the wire used to fabricate the coil. The self-inductance is

$$L = \frac{\mu\pi^2 N^2 a}{l} \quad (H) \qquad (31)$$

where l is the length of the coil. In the free space, the magnetic field strength generated by a coil antenna in the near field is [28]:

$$H_0 = \frac{Na^2 I}{2(a^2+z^2)^{3/2}} \quad (A/m) \qquad (32)$$

The magnetic field magnitude for a lossy medium is then $H = H_0 exp(-\alpha z)$ according to (29). This magnetic field induces a voltage in the tag's coil antenna, given by:

$$U_2 = -N_2 \frac{d\Phi_{21}}{dt} = -M \frac{di_1}{dt} \qquad (33)$$

where $\Phi_{21} = \int \mathrm{b}B \cdot d\boldsymbol{S}$ is the magnetic flux through each turn, $\boldsymbol{B} = \mu \boldsymbol{H}$ the magnetic field and **S** the surface area of the coil. Considering that the reader's and tag's coils are aligned, and using (32):

$$B_z = \left(\frac{\mu N a_1^2 I}{2\left(a_1^2+z^2\right)^{2/3}} \right) e^{-\alpha z} \qquad (34)$$

Therefore, the mutual inductance $M = k\sqrt{L_1 L_2}$ is:

$$M = \left(\frac{\mu \cdot \pi \cdot N_1 \cdot a_1^2 \cdot N_2 \cdot a_2^2}{2 \cdot \left(a_1^2+z^2\right)^{3/2}} \right) \cdot e^{-\alpha z} \qquad (35)$$

where α is the attenuation constant of the medium.

The transmission power can be defined as the power consumed by the radiation resistance in the reader (transmitter) antenna:

$$P_{TX} = \frac{1}{2} Re(Z_{11}) \cdot |I_1|^2 \qquad (36)$$

The received power is defined as the power consumed in the load:

$$P_{RX}(z) = \frac{1}{2} Re(Z_L) \cdot |I_2|^2 \qquad (37)$$

Using (30) and considering $Z_S \approx 0$, the received power can be written as:

$$P_{RX}(z) = P_{TX} \frac{Re(Z_L)\omega^2 M^2}{Re(Z_{TX})|Z_L+Z_{RX}|^2} \qquad (38)$$

Path loss in decibels (dB) can be defined as:

$$PL = -10 \log_{10} \left(\frac{P_{RX}}{P_{TX}} \right) (dB) \qquad (39)$$

The path loss is a function of the number of turns and radius of both coils and the impedances of the system, as well as the frequency and the distance between reader and tag. The highest amount of power is transferred to the load when its impedance is matched with the impedance of the antenna.

The path loss for the MI system increases with the increasing distance between reader and tag. Also, the path loss is higher for seawater due to the higher conductivity of the medium. As the frequency increases, the distance from the reader where the border between the near and the far-field is located decreases. This implies that the maximum theoretical range decreases with frequency. We can then conclude that there is an optimal combination of frequency and distance for each application. In addition to that, the attenuation factor α is higher for higher frequencies.

The influence of the number of turns of the transmitter or the receiver coil in the mutual inductance M is linear. Therefore, the power received would increase quadratically with the increase in the number of turns. However, it also increases the energy losses in the internal resistance of the coil as it increases. It is also worth noting that a bigger coil diameter allows for more magnetic flux to pass through, but it also has the effect of increasing the internal resistance of the coil.

A more in-depth model of underwater magnetic induction communication can be found in [15]. The model shown here assumes that the reader and tag coils are oriented in the same direction, with the field strength reaching zero if the angle between coils is 90°. To remove this limitation, the authors in [48] present a model of the Underwater MI channel for a tri-directional coil. To increase the achievable range of MI systems, waveguides can be used [14][49]. The authors in

2020, © Copyright by authors, Published under agreement with IARIA - www.iaria.org

[17] provide a different but similar model that is based on the quality factor of the coil inductor.

1) Data transmission from tag

When a transponder is located in the magnetic alternating field generated by the reader, the reader 'sees' the transponder as the secondary wing of the transformer. This means that the transponder's impedance is reflected back to the reader as the *transformer impedance* Z_T.

If the transponder antenna impedance changes, this is reflected back to the reader's coil via the reflected impedance Z_T . Therefore, a data stream can be transmitted via modulation of the voltage Z_L in the reader's coil (called *Load Modulation*); this can be demodulated by the reader via rectification of the voltage [28]. This is only feasible in the near-field as if the transponder leaves the appropriate read range, the coupling is lost and the transmission link is not operational anymore.

For an amplitude modulating system, due to the weak coupling between reader and transponder antennas, the voltage fluctuation is orders of magnitude smaller than the voltage provided by the reader. As a direct result, the reader has to integrate a complex circuitry to separate noise from the signal and detect the data stream. On the other hand, if the transponder modulates the signal at a frequency f_s, smaller than the frequency of the magnetic field (f_0), two spectral lines $\pm f_s$ are created and they can be filtered with a band-pass filter and demodulated more easily [47].

B. Far-field

In the far-field, the electromagnetic fields separate completely from the reader's antenna and become propagating waves, no longer retroacting upon the reader's antenna. These waves are captured by the antenna on the transponder. The energy on the antenna is rectified and used to power up the IC. The frequency range commonly used for this type of transmission is the Ultra-High Frequency (UHF) and Microwave.

A linearly polarized plane EM wave propagating in lossy media in the z-direction can be described by the electric field strength E_x:

$$E_x = E_0 e^{j\omega t - \gamma z} \qquad (40)$$

with $\gamma = \alpha + j\,\omega\beta$ as the propagating constant according to (5) and (6).

The radiation power density *S* is the instantaneous value of the Poynting vector **S**=**E**×**H**. From [31] and considering (29):

$$\boldsymbol{S} = \frac{1}{2} Re(\boldsymbol{E} \times \boldsymbol{H}) = \hat{\boldsymbol{a}}_{\boldsymbol{z}} \frac{|E_0|}{2} e^{-2\alpha z} Re\left(\frac{1}{\eta_c^*}\right) \qquad (41)$$

where η_C is the intrinsic impedance of the medium, given by (42).

$$\eta_C = \sqrt{\frac{j\omega\mu}{\sigma + j\omega\varepsilon}} \qquad (42)$$

For the transmitting antenna in the free-space, s_0 is the power supplied to it over the area of the spread surface:

$$S_0 = \frac{P_{EIRP}}{4\pi z^2} = \frac{P_{TX} G_{TX}}{4\pi z^2} \qquad (43)$$

Whereas the radiation power density in a lossy medium is then:

$$S = S_0 e^{-2\alpha z} \qquad (44)$$

For the receiving antenna, the average power received is the radiation power density times its effective receiving area A_e [45]:

$$P_{RX} = S \cdot A_e = S \cdot \frac{G_{RX}\lambda^2}{4\pi} \qquad (45)$$

The transmission equation then can be written as:

$$P_{RX} = P_{TX}\left(\frac{G_{TX} G_{RX} \lambda^2}{(4\pi z)^2}\right) e^{-2\alpha z} \qquad (46)$$

where G_{TX} and G_{RX} are the antenna gains for transmitter and receiver respectively, λ=(2π)/β is the wavelength and *z* is the distance between antennas. This equation assumes that the antennas are aligned and have the same polarization. The path loss PL_{EM} in decibels is then defined as $PL_{EM} = -10\log_{10}(P_{RX}/P_{TX})$.

1) Data transmission from tag

For passive RFID, the method of transmitting back to the reader is via *Backscatter*. Electromagnetic waves are reflected by objects that are larger than half the wavelength ($\lambda/2$) [28]. The efficiency of this reflection depends on the radar cross-section of the object: antennas that are resonant with the waves have a larger reflection cross-section. The reflection characteristics can be altered by changing the load that is connected to the antenna. For example, if a load R_L is switched on and off while connected to the antenna, this changes the reflection characteristics of the antenna, generating a modulated backscatter signal [28]. The range is limited by the amount of energy that reaches the tag (path loss) and the sensitivity of the reader's receiver to the reflected signal (reflected signal strength $\propto 1/x^4$) [50]. The authors in [51] present a method for measuring the backscatter of an RFID tag and for calculating its radar cross-section. They utilise a network analyser connected to an anechoic chamber.

2020, © Copyright by authors, Published under agreement with IARIA - www.iaria.org

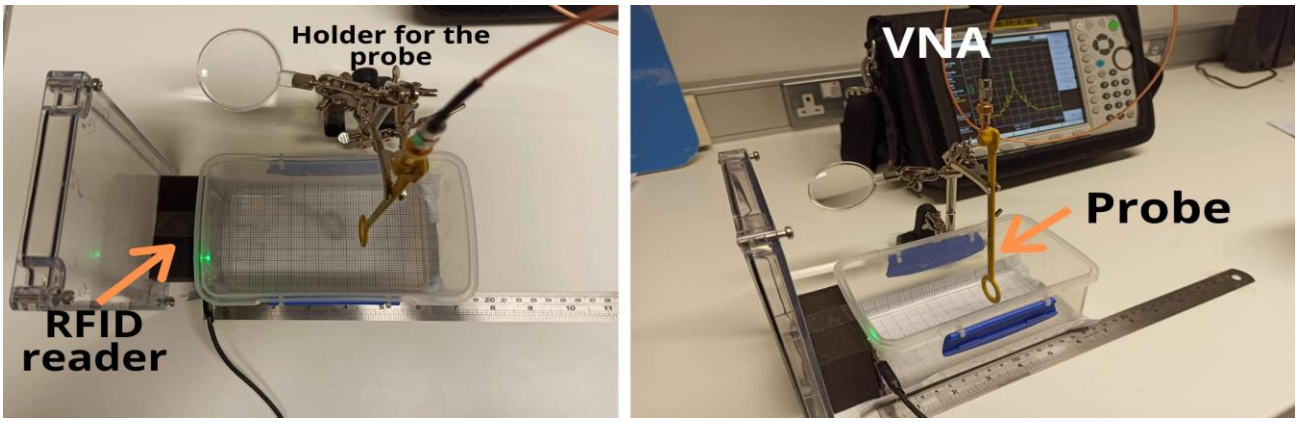


Figure 7: Experimental setup for measuring the magnetic field strength consisting of a plastic container, magnetic probe, holder and stand for the probe and VNA. Each RFID reader system was placed and secured on the side of the plastic container.

V. MEASUREMENTS

To explore the difference in magnetic field strength between free-space and water in the near-field region, a preliminary experiment was designed. The Anritsu MS2038C VNA Master [52] vector network analyser and the probe 100C from Beehive Electronics, USA [53] were used to measure the magnetic field strength at the system's resonant frequency. Two Evaluation Kit RFID readers were used: *MRD2EVM* from Texas Instruments, USA that operates at 134.2 kHz [54] and *Pepper Wireless C1 USB* from Eccel Technology Ltd, UK that operates at 13.56 MHz [55]. Both have square loop antennae embedded on the printed circuit board, with sides of length 3.0 cm and 4.5 cm, and number of turns 14 and 3, respectively.

For a square loop antenna with *N*-turns, the magnetic field strength in free-space can be written as [56]:

$$H_0 = \frac{NI}{2\pi\left(\frac{z^2}{l^2}+\frac{1}{4}\right)\sqrt{z^2+\frac{l^2}{2}}} \quad (47)$$

where *z* is the distance from the centre of the antenna and *l* is the length of the side of the antenna. Using (29), for a lossy medium (in this case saline water), the magnetic field strength is then

$$H = H_0 exp(-\alpha z) \quad (48)$$

Using α from (5) with the salinity and frequency, we can then calculate the theoretical values for the magnetic field strength for any distance and compare this with the measurements made with the probe.

For both systems, the setup for the experiments was the same, as seen in Figure 7. The readers were placed and secured on the side of a plastic transparent container. The probe was placed in different distances *z* from the centre of the embedded antenna of the reader. A measurement ruler and grid paper were used for the precise placement of the probe. The free-space tests were done without water inside the container. For the other measurements, the probe was submerged in the water solution to get the measured field strength.

For the experimental test, 4 water solutions were used, named as: distilled water, freshwater, brackish water, and saline water. The water solutions were prepared as follows. First the container was placed in a scale, and the mass of NaCl was added, according to the target value of salinity for each solution. Then, distilled water was added until the whole solution mass reached 700g (the volume of the plastic container used for the experiments). Table III shows the mass of salt for each solution and their salinity and calculated conductivity.

TABLE III. SOLUTIONS USED FOR THE EXPERIMENT, TEMPERATURE AT WHICH THEY WHERE MIXED, THEIR SALINITY AND CALCULATED CONDUCTIVITY FOR EACH SOLUTION ACCORDING TO [44].

Solution	NaCl mass	Total mass	Salinity	Tempe-rature	Calculated Conductivity (at 1 MHz)
Freshwater	0.35 g	0.7002 kg	0.499 g/kg	19 C	0.093 S/m
Brackish Water	10.5 g	0.7003 kg	14.99 g/kg	18 C	2.32 S/m
Saline Water	24.5 g	0.7003 kg	34.98 g/kg	19 C	5.04 S/m

For each solution, the probe was placed and held at different distances from the centre of the antenna and the peak value of the magnetic field was measured using the VNA. After this was done, the probe was wiped so there was no contamination between solutions.

The output power values measured by the probe P_{out} were then converted from *dBm* to magnetic field strength in *A/m* using the probe manufacturer's guidelines [53], using Equations (49) and (50), where f_{MHz} is the frequency of the system in *MHz*, B_{out} is the magnetic flux density, and H_{out}

2020, © Copyright by authors, Published under agreement with IARIA - www.iaria.org

is the magnetic field strength. The raw data collected from the probe and the VNA in *dBm* can be found in Tables IV and V.

$$20 \times log_{10}(B_{out}) = P_{out} - 42.2 - 20 \times log_{10}(f_{MHz}) \quad (49)$$

$$H_{out} = \frac{10^{B}}{\mu} \quad (A/m) \quad (50)$$

Figure 8 shows the measured values of magnetic field strength for the 134.2 kHz system, while Figure 9 shows the values for the 13.56MHz system.

Figures 10 and 11 show the comparison between measured values of field strength and the theoretical values expected using a calculated α from the water salinity. For this, the peak current (A) flowing through the antennas was measured under the same experimental conditions, and Equation (47) was used.

TABLE IV. MEASURED VALUES OF P_{out} IN DBM FOR THE 134.4KHZ SYSTEM FOR FREE-SPACE (FREE), DISTILLED WATER (DW), FRESHWATER (FW), BRACKISH WATER (BW) AND SALINE WATER (SW) SOLUTIONS.

z (cm)	F (dBm)	DW (dBm)	FW (dBm)	BW (dBm)	SW (dBm)
0.2	-2.2	-2.18	-2.63	-3.62	-1.96
1	-9.66	-7.68	-6.84	-8.34	-7.35
2	-13.82	-14.24	-13.36	-15.42	-14.13
3	-20.2	-21.13	-19.6	-21.06	-20.22
4	-26.1	-25.95	-25.41	-25.81	-25.72
5	-30.15	-30.69	-30.27	-30.04	-30.43
6	-34.02	-34.44	-33.41	-34.06	-34.16
7	-37.7	-37.36	-36.75	-37.24	-37.3
8	-40.9	-40.76	-40.42	-40.56	-40.79
9	-43.34	-43.66	-42.79	-43.07	-43.26
10	-45.65	-45.66	-45.31	-45.84	-45.9

TABLE V. MEASURED VALUES OF P_{out} IN DBM FOR THE 13.56MHZ SYSTEM FOR FREE-SPACE (F), DISTILLED WATER (DW), FRESHWATER (FW), BRACKISH WATER (BW) AND SALINE WATER (SW) SOLUTIONS.

z (cm)	F (dBm)	DW (dBm)	FW (dBm)	BW (dBm)	SW (dBm)
0.2	11.64	11.09	11.03	10.7	9.49
1	7.72	7.96	7.87	6.65	6
2	2.74	2.32	2.58	1.73	1.24
3	-2.37	-2.12	-2.06	-3.84	-4.15
4	-6.92	-7.06	-7.01	-7.94	-8.53
5	-10.92	-11.56	-10.76	-11.95	-12.75
6	-14.33	-15.02	-14.92	-15.63	-16.7
7	-17.76	-17.94	-17.56	-18.28	-19.74
8	-20.56	-20.52	-20.88	-21.65	-22.76
9	-23.26	-23.76	-23.66	-24.12	-25.51
10	-25.76	-25.66	-25.96	-26.6	-27.76

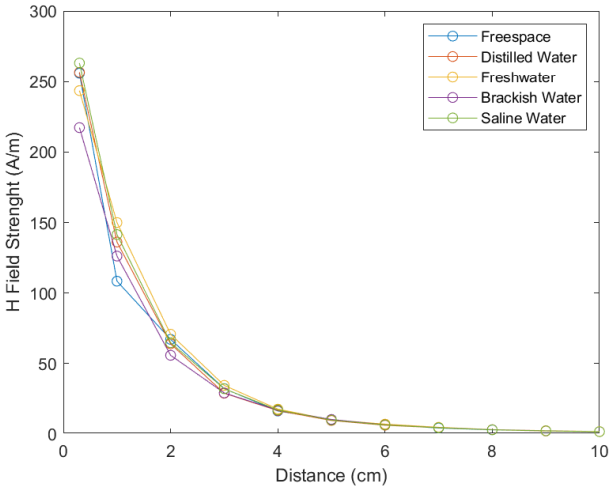


Figure 8: Measured magnetic field strength values for the Texas Instruments MRD2EVM evaluation kit (*f*=134.2 kHz).

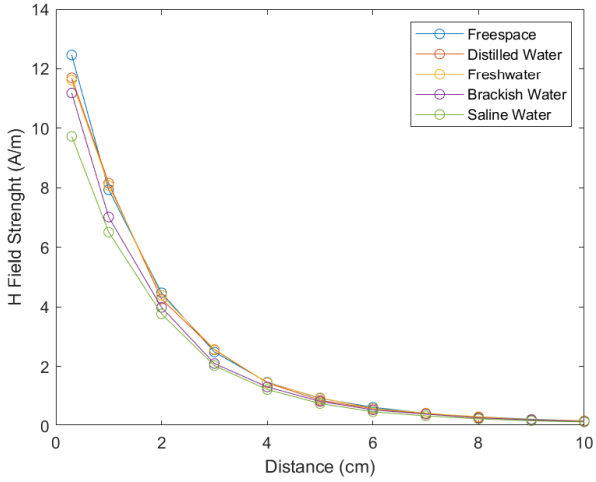


Figure 9: Measured magnetic field strength values for the Eccel Technology Pepper C1 USB evaluation kit (*f*=13.56 MHz).

VI. DISCUSSIONS

The most common method of wireless transmission underwater is acoustic communication. This is due to the long range that can be accomplished with this technology. However, some applications do not need such long range and are deeply affected by acoustic noise and refractions, reflections and multipath due to the proximity to the water surface, such as coastal environments. In these cases, wireless communication can be better served by other methods that do not suffer from these problems. We explore the possibility of using RFID technology to better serve these environments.

2020, © Copyright by authors, Published under agreement with IARIA - www.iaria.org

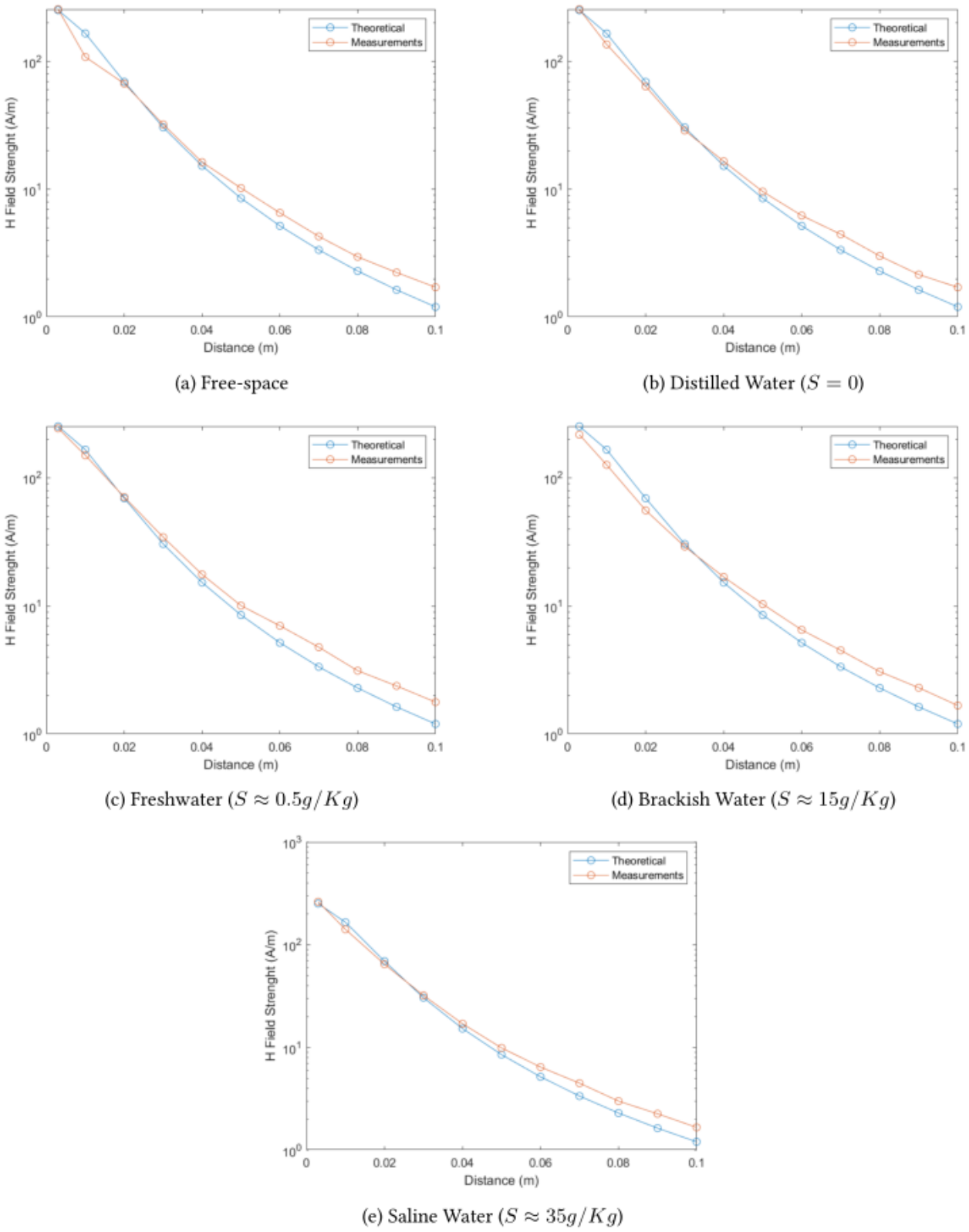


Figure 10: Comparison between measured values of magnetic field strength for different salinity values underwater for the 134.2kHz system.

2020, © Copyright by authors, Published under agreement with IARIA - www.iaria.org

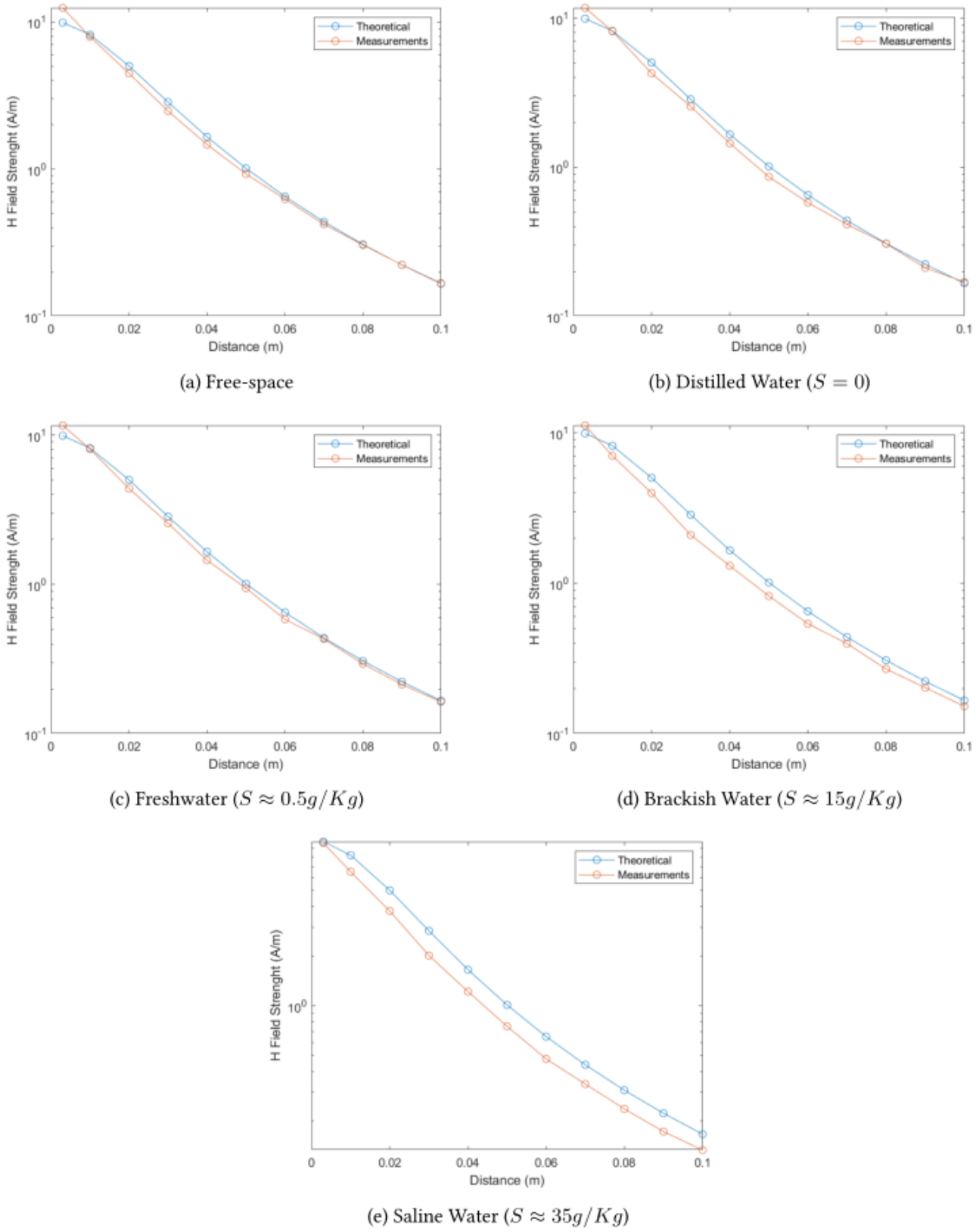


Figure 11: Comparison between measured values of magnetic field strength for different salinity values underwater for the 13.56MHz system.

2020, © Copyright by authors, Published under agreement with IARIA - www.iaria.org

In the near-field region, the magnetic component of the electromagnetic field dominates. The method of communication for RFID in this region is MI. Compared to other methods of underwater communications, MI has several advantages. It is not affected by multipath propagation or fading and the magnetic field can cross the water to air boundary with low attenuation [14]. The signal propagation delay is negligible if compared to acoustic waves. The channel response is predictable, and a sufficiently large range can be achieved with modest data rates [13].

For the far-field, the electromagnetic field propagates as a wave, and the communication is realized through radiofrequency. Due to the high attenuation, there is a severe constraint on data rates and propagation distances for this method [2]. Lower frequency signals have lower attenuation (due to conductivity of the water) but require larger antennas. This also limits the bandwidth of the system due to the lower frequency of operation. Higher frequency systems would then require more power to reach the same ranges. Shallow water environments, in particular, pose a problem to wave propagation due to the proximity to the water/air upper boundary and to the river/sea bed, which causes multipath propagation [5][6].

Both technologies do not require line-of-sight and are unaffected by light and acoustic ambient noise. Moreover, the channel response is independent of water quality conditions, such as turbidity. The literature generally agrees that the achievable range for a given transmission power is not great for both MI and RF. The reasoning is due to the high attenuation caused by the medium conductivity which increases with the salinity of the water. From this, it follows that long-range transmissions underwater, particularly in a marine environment, are best served by acoustic communication based systems [2].

However, there are some evidence that this attenuation could be lower than expected. The authors in [57] managed to transmit a RF signal at 90 m distance in seawater with a lower attenuation than expected. To reflect this results, [45] propose the change in the attenuation factor α to α' according to Equation (27). In addition to that, the dielectric permittivity for saline water is not completely understood [34]. There are models available extrapolated from measurement data, but they do not agree completely. Since the dielectric permittivity affects the attenuation, it follows that the attenuation itself could have a different value.

The results from our experiment in Figure 10 for the 134.2 kHz system show that there is a difference between the expected theoretical value and the measured value, especially as the distance increases. Yet, the same cannot be said for the results in Figure 11 for the 13.56 MHz system. In this latter case, the measurements seem to be lower than the expected value. It is not clear what is the cause, but this suggests that higher frequencies suffer higher attenuation in a manner not considered in the model.

As expected, a higher water salinity implies in a higher attenuation for the signal. Although the relative permittivity for seawater is slightly smaller than for freshwater, as can be observed in Figure 3, the conductivity for seawater is higher (see Figure 2) and dominates, increasing the attenuation factor. It is also worth noting that the 134.2 kHz system is not as affected by the increasing salinity of water as the 13.56 MHz system, as it can be seen looking at the values in Tables IV and V. This means that a MI communication system for a marine environment should be designed with a lower frequency, keeping in mind the needed bandwidth to transmit data and other requirements. This would ensure that the system is efficient, as there is lower energy being lost in the transmission.

Some authors argue that MI has a lower attenuation than RF for freshwater, and similar results for seawater [14]. This fact, combined with its immunity to multipath and fading, implies that MI could be a great alternative for wireless communications underwater. In addition, the achievable range of MI communications can be greatly extended by deploying waveguides that do not require power – simple passive relay coils that guide the magnetic field – such as demonstrated in [14][49]. For example, [14] uses an MI waveguide and achieves a range 26 times higher than a normal MI system. Another development that improves MI communications underwater is to use omnidirectional coils that remove the requirement of the transmitting and receiving coils being aligned [13][48].

However, to design an underwater RFID system it is required to balance a trade-off between range, transmission power and frequency (and therefore data rate and channel capacity). Nonetheless, the RFID system can always be engineered to achieve the best range given its power budget.

For an MI system, the size and number of turns of the transmitting and receiving coils also has an impact on the path loss. A bigger coil diameter increases the generated and captured magnetic flux for the transmitter/reader and receiver/tag, which increases the mutual induction and decreases the path loss. However, this is also a trade-off, as a bigger coil has a bigger internal resistance, requiring more power to transmit. It is also worth noting that some applications have size restrictions.

In the far-field category, the antenna can be carefully designed to provide the best radar cross-section, and therefore antenna gain, for the desired application. Again, the size of the antenna is important, as it is related to the wavelength. There is also a trade-off to be made for the frequency, attenuation, and antenna size: for a lower attenuation, the system would need a lower frequency, which requires a bigger antenna.

An example application that would benefit from MI communication over acoustic would be sensors deployed in coastal areas and fish farms [58]. In these environments, the acoustic noise – from waves, animal life and vessels – and the proximity with the water surface negatively impact acoustic underwater communications. In such scenarios, MI underwater communication would better fulfil the communication mechanisms for the of the system.

2020, © Copyright by authors, Published under agreement with IARIA - www.iaria.org

VII. Conclusion and Future Work

Given the existing challenges in wireless underwater communications, it is worth exploring alternatives, such as RFID. However, underwater RFID communication is not a well-explored topic in the scientific community. In this paper, we expanded on the existing theoretical model for RFID channel characteristics to account for the attenuation that the electromagnetic field suffers underwater. The water salinity is an important factor, which is used to calculate the dielectric permittivity and the conductivity of the water, and therefore, the attenuation. The RFID operation was separated into two categories: near-field and far-field. For both cases, the physical characteristics of the transmission were presented and from this, the equation for path loss was obtained.

In both technologies, the water salinity is a problem, as it increases the conductivity of the medium and, therefore, its attenuation of RFID signals. However, MI communication has advantages over RF in terms of immunity to multipath propagation and fading. In addition, a magnetic field can cross the air/water boundary, which is required for some applications. Therefore, near-field RFID communication is a promising alternative for underwater wireless communications.

The model presented in this paper considers that both the transmitting and receiving antennas are located underwater with no transition borders and other losses. This model could be expanded to account for transition borders such as the air-water interface located at the water surface or the interface with the waterproofing material of the reader and tag.

In this paper, we presented measurements for magnetic field strength for two near-field systems in different water salinity conditions. The results for the 134.2 kHz show that the attenuation may not be as strong as expected, especially for higher distances. But the results for the 13.56 MHz follow more closely the expected values, sometimes being even lower. This seems to imply that there may be a relationship between the attenuation factor and the frequency that is not currently expressed in the model. More experimental data is needed to draw any significant conclusions.

The results also suggest that a higher concentration of salt in the water increases the attenuation, which agrees with the model. However, the effect is more prominent the higher the frequency, which implies that the best communications solution for marine environments requires the use of lower frequencies to minimise attenuation.

Acknowledgment

This work is part of IMPAQT (https://impaqtproject.eu/) – This project has received funding from the European Union's Horizon 2020 research and innovation programme under Grant Agreement No 774109. Aspects of this publication have emanated from research conducted with the financial support of Science Foundation Ireland (SFI) and is co-funded under the European Regional Development Fund under Grant Numbers 13/RC/2077 (CONNECT), 12/RC/2289-P2 (INSIGHT) and 16/RC/3835 (VISTAMILK).

References

[1] C. Peres, J. Buckley, N. N. Rather, and B. O'Flynn, 'Theoretical models for underwater RFID', in *SENSORCOMM 2019*, Nice, France, Oct. 2019, pp. 80–88, Accessed: Sep. 01, 2020. [Online]. Available: https://cora.ucc.ie/handle/10468/9642.

[2] C. M. G. Gussen, P. S. R. Diniz, M. L. R. Campos, W. A. Martins, F. M. Costa, and J. N. Gois, 'A Survey of Underwater Wireless Communication Technologies', *JCIS*, vol. 31, no. 1, Art. no. 1, 2016, doi: 10.14209/jcis.2016.22.

[3] J. Heidemann, Wei Ye, J. Wills, A. Syed, and Yuan Li, 'Research challenges and applications for underwater sensor networking', in *IEEE Wireless Communications and Networking Conference, 2006. WCNC 2006.*, Las Vegas, NV, USA, 2006, pp. 228–235, doi: 10.1109/WCNC.2006.1683469.

[4] M. C. Domingo, 'An overview of the internet of underwater things', *Journal of Network and Computer Applications*, vol. 35, no. 6, Art. no. 6, Nov. 2012, doi: 10.1016/j.jnca.2012.07.012.

[5] L. Lambo, Z. Shengli, and C. Jun-Hong, 'Prospects and problems of wireless communication for underwater sensor networks', *Wireless Communications and Mobile Computing*, vol. 8, no. 8, Art. no. 8, Oct. 2008, doi: 10.1002/wcm.654.

[6] X. Che, I. Wells, G. Dickers, P. Kear, and X. Gong, 'Re-evaluation of RF electromagnetic communication in underwater sensor networks', *IEEE Communications Magazine*, vol. 48, no. 12, Art. no. 12, Dec. 2010, doi: 10.1109/MCOM.2010.5673085.

[7] Y. Li, S. Wang, C. Jin, Y. Zhang, and T. Jiang, 'A Survey of Underwater Magnetic Induction Communications: Fundamental Issues, Recent Advances, and Challenges', *IEEE Communications Surveys Tutorials*, vol. 21, no. 3, Art. no. 3, thirdquarter 2019, doi: 10.1109/COMST.2019.2897610.

[8] A. Pozzebon, 'Bringing near field communication under water: short range data exchange in fresh and salt water', in *2015 International EURASIP Workshop on RFID Technology (EURFID)*, Oct. 2015, pp. 152–156, doi: 10.1109/EURFID.2015.7332401.

[9] D. Bertoni, G. Sarti, G. Benelli, A. Pozzebon, and G. Raguseo, 'Radio Frequency Identification (RFID) technology applied to the definition of underwater and subaerial coarse sediment movement', *Sedimentary Geology*, vol. 228, no. 3, Art. no. 3, Jul. 2010, doi: 10.1016/j.sedgeo.2010.04.007.

[10] E. B. Thorstad, A. H. Rikardsen, A. Alp, and F. Økland, 'The Use of Electronic Tags in Fish Research – An Overview of Fish Telemetry Methods', *Turkish Journal of Fisheries and Aquatic Sciences*, vol. 13, no. 5, Art. no. 5, 2013.

[11] S. J. Cooke, S. G. Hinch, M. C. Lucas, and M. Lutcavage, 'Biotelemetry and Biologging', in *Fisheries Techniques*, 3rd edition., American Fisheries Society, 2012, pp. 819–860.

[12] G. Benelli and A. Pozzebo, 'RFID Under Water: Technical Issues and Applications', in *Radio Frequency Identification from System to Applications*, M. I. B. Reaz, Ed. InTech, 2013.

2020, © Copyright by authors, Published under agreement with IARIA - www.iaria.org

[13] I. F. Akyildiz, P. Wang, and Z. Sun, 'Realizing underwater communication through magnetic induction', *IEEE Communications Magazine*, vol. 53, no. 11, Art. no. 11, Nov. 2015, doi: 10.1109/MCOM.2015.7321970.

[14] M. C. Domingo, 'Magnetic Induction for Underwater Wireless Communication Networks', *IEEE Transactions on Antennas and Propagation*, vol. 60, no. 6, Art. no. 6, Jun. 2012, doi: 10.1109/TAP.2012.2194670.

[15] B. Gulbahar and O. B. Akan, 'A Communication Theoretical Modeling and Analysis of Underwater Magneto-Inductive Wireless Channels', *IEEE Transactions on Wireless Communications*, vol. 11, no. 9, Art. no. 9, Sep. 2012, doi: 10.1109/TWC.2012.070912.111943.

[16] Z. Sun and I. F. Akyildiz, 'Magnetic Induction Communications for Wireless Underground Sensor Networks', *IEEE Transactions on Antennas and Propagation*, vol. 58, no. 7, Art. no. 7, Jul. 2010, doi: 10.1109/TAP.2010.2048858.

[17] U. Azad, H. C. Jing, and Y. E. Wang, 'Link Budget and Capacity Performance of Inductively Coupled Resonant Loops', *IEEE Transactions on Antennas and Propagation*, vol. 60, no. 5, Art. no. 5, May 2012, doi: 10.1109/TAP.2012.2189696.

[18] H. Nguyen, J. I. Agbinya, and J. Devlin, 'Channel Characterisation and Link Budget of MIMO Configuration in Near Field Magnetic Communication', *International Journal of Electronics and Telecommunications*, vol. 59, no. 3, Art. no. 3, Sep. 2013, doi: 10.2478/eletel-2013-0030.

[19] D. Gawade *et al.*, 'A battery-less NFC sensor transponder for museum artefact monitoring - a review of NFC sensor technology and a proposed solution', in *SENSORCOMM 2019*, Nice, France, Oct. 2019, pp. 89–96, Accessed: Sep. 01, 2020. [Online]. Available: https://cora.ucc.ie/handle/10468/9634.

[20] STMicroelectronics, 'ST25DV04K- Datasheet'. 2018, Accessed: Aug. 01, 2020. [Online]. Available: https://www.st.com/resource/en/datasheet/st25dv04k.pdf.

[21] D. Sen, P. Sen, and A. M. Das, *RFID for energy & utility industries*. Pennwell Books, 2009.

[22] S. A. Weis, 'RFID (radio frequency identification): Principles and applications', *System*, vol. 2, no. 3, pp. 1–23, 2007.

[23] 'ISO/IEC 18000-2:2009 Information technology — Radio frequency identification for item management — Part 2: Parameters for air interface communications below 135 kHz'. [Online]. Available: https://www.iso.org/standard/46146.html.

[24] 'ISO/IEC 18000-3:2010 Information technology — Radio frequency identification for item management — Part 3: Parameters for air interface communications at 13.56 MHz'. [Online]. Available: https://www.iso.org/standard/53424.html.

[25] 'ISO/IEC 15693-1:2010 Identification cards — Contactless integrated circuit cards — Vicinity cards — Part 1: Physical characteristics'. [Online]. Available: https://www.iso.org/standard/39694.html.

[26] 'ISO/IEC 14443-1:2018 Cards and security devices for personal identification — Contactless proximity objects — Part 1: Physical characteristics'. [Online]. Available: https://www.iso.org/standard/73596.html.

[27] E. C. M. Association, *ECMA340–Near Field Communication Interface and Protocol (NFCIP-1)*. Genf, 2004.

[28] K. Finkenzeller, *RFID Handbook: fundamentals and applications in contactless smart cards, radio frequency identification and near-field communication*. Hoboken, N.J.: Wiley, 2014.

[29] P. Haigh, M. Hayes, D. Gawade, and B. O'Flynn, 'Towards autonomous smart sensing systems', in *2020 IEEE International Instrumentation and Measurement Technology Conference (I2MTC)*, 2020, pp. 1–6.

[30] Texas Instrument, 'Antenna Design Guide for the TRF79xxA'. Accessed: Aug. 01, 2020. [Online]. Available: http://www.ti.com/lit/an/sloa241b/sloa241b.pdf.

[31] C. A. Balanis, *Advanced engineering electromagnetics*, 2nd ed. Hoboken, N.J: John Wiley & Sons, 2012.

[32] E. E. Kriezis, T. D. Tsiboukis, S. M. Panas, and J. A. Tegopoulos, 'Eddy currents: theory and applications', *Proceedings of the IEEE*, vol. 80, no. 10, pp. 1559–1589, Oct. 1992, doi: 10.1109/5.168666.

[33] P. Fofanoff and R. C. Millard Jr, 'UNESCO, Algorithms for computation of fundamental properties of seawater, UNSESCO Tech. Pap', *Marine Science*, no. 44, p. 55.

[34] R. Somaraju and J. Trumpf, 'Frequency, Temperature and Salinity Variation of the Permittivity of Seawater', *IEEE Transactions on Antennas and Propagation*, vol. 54, no. 11, Art. no. 11, Nov. 2006, doi: 10.1109/TAP.2006.884290.

[35] P. J. W. Debye, *Polar molecules*. Chemical Catalog Company, Incorporated, 1929.

[36] D. R. Lide, 'Handbook of Chemistry and Physics, CRC Press', *Boca Raton, FL*, vol. 1, no. 993, p. 1, 1993.

[37] J. B. Hasted, S. K. Husain, F. A. M. Frescura, and J. R. Birch, 'The temperature variation of the near millimetre wavelength optical constants of water', *Infrared physics*, vol. 27, no. 1, pp. 11–15, 1987.

[38] A. P. Stogryn, H. T. Bull, K. Rubayi, and S. Iravanchy, 'The microwave permittivity of sea and fresh water', *GenCorp Aerojet, Azusa, CA*, 1995.

[39] D. G. Archer and P. Wang, 'The dielectric constant of water and Debye-Hückel limiting law slopes', *Journal of physical and chemical reference data*, vol. 19, no. 2, pp. 371–411, 1990.

[40] H. J. Liebe, G. A. Hufford, and T. Manabe, 'A model for the complex permittivity of water at frequencies below 1 THz', *International Journal of Infrared and Millimeter Waves*, vol. 12, no. 7, pp. 659–675, 1991.

[41] T. Meissner and F. J. Wentz, 'The complex dielectric constant of pure and sea water from microwave satellite observations', *IEEE Transactions on Geoscience and Remote Sensing*, vol. 42, no. 9, pp. 1836–1849, 2004.

[42] L. Klein and C. Swift, 'An improved model for the dielectric constant of sea water at microwave frequencies', *IEEE Transactions on Antennas and Propagation*, vol. 25, no. 1, pp. 104–111, 1977.

[43] A. Stogryn, 'Equations for calculating the dielectric constant of saline water (correspondence)', *IEEE Transactions on Microwave Theory and Techniques*, vol. 19, no. 8, pp. 733–736, 1971.

[44] 'Recommendation ITU-R P.527-5'. International Telecommunication Union, 2019, Accessed: Aug. 01, 2020. [Online]. Available: https://www.itu.int/rec/R-REC-P.527-5-201908-I/en.

2020, © Copyright by authors, Published under agreement with IARIA - www.iaria.org

[45] C. Uribe and W. Grote, 'Radio Communication Model for Underwater WSN', in *2009 3rd International Conference on New Technologies, Mobility and Security*, Dec. 2009, pp. 1–5, doi: 10.1109/NTMS.2009.5384789.

[46] C. A. Balanis, *Antenna theory: analysis and design*, 3rd ed. Hoboken, NJ: John Wiley, 2005.

[47] H. Lehpamer, *RFID design principles*, 2nd ed. Boston: Artech House, 2012.

[48] H. Guo, Z. Sun, and P. Wang, 'Channel Modeling of MI Underwater Communication Using Tri-Directional Coil Antenna', in *2015 IEEE Global Communications Conference (GLOBECOM)*, Dec. 2015, pp. 1–6, doi: 10.1109/GLOCOM.2015.7417399.

[49] Z. Sun, I. F. Akyildiz, S. Kisseleff, and W. Gerstacker, 'Increasing the Capacity of Magnetic Induction Communications in RF-Challenged Environments', *IEEE Transactions on Communications*, vol. 61, no. 9, Art. no. 9, Sep. 2013, doi: 10.1109/TCOMM.2013.071813.120600.

[50] R. Want, 'RFID Explained: A Primer on Radio Frequency Identification Technologies', *Synthesis Lectures on Mobile and Pervasive Computing*, vol. 1, no. 1, Art. no. 1, Jan. 2006, doi: 10.2200/S00040ED1V01200607MPC001.

[51] K. V. S. Rao and P. V. Nikitin, 'Theory and measurement of backscattering from RFID tags', *IEEE Antennas and Propagation Magazine*, vol. 48, no. 6, Art. no. 6, Dec. 2006, doi: 10.1109/MAP.2006.323323.

[52] 'VNA master MS20xxC technical data sheet', manual, Aug. 2019.

[53] '100 Series EMC Probes - Datasheet', Beehive Electronics, 100C, 2005.

[54] 'HDX RFID Reader System – Microreader RI-STU-MRD2', manual SCBU049, Aug. 2012.

[55] 'Pepper C1 user manual', manual SKU000395, Sep. 2019.

[56] G. D. Durgin, 'ECE 3065 notes', TESSAL - Georgia Institute of Technology, manual.

[57] A. Shaw, A. I. Al-Shamma'a, S. R. Wylie, and D. Toal, 'Experimental investigations of electromagnetic wave propagation in seawater', in *2006 European Microwave Conference*, 2006, pp. 572–575.

[58] 'IMPAQT Project'. https://impaqtproject.eu/about-impaqt/ (accessed Sep. 01, 2020).

2020, © Copyright by authors, Published under agreement with IARIA - www.iaria.org